



# Development and Occurrence Mechanisms of Fault-Slip Rockburst in a Deep Tunnel Excavated by Drilling and Blasting: A Case Study

Wei Zhang<sup>1</sup> · Xia-Ting Feng<sup>1</sup> · Zhi-Bin Yao<sup>1</sup> · Lei Hu<sup>1</sup> · Ya-Xun Xiao<sup>2</sup> · Guang-Liang Feng<sup>2</sup> · Wen-Jing Niu<sup>1</sup> · Yu Zhang<sup>1</sup>

Received: 9 November 2021 / Accepted: 10 May 2022 / Published online: 23 June 2022  
© The Author(s), under exclusive licence to Springer-Verlag GmbH Austria, part of Springer Nature 2022

## Abstract

In this work, an extremely intense fault-slip rockburst case, with a local magnitude of 2.3, observed in a deep tunnel in southwestern China was introduced as a case study. The rockburst caused a large economic loss and delayed the construction schedule for nearly 2 months. In-situ failure analysis, geological surveys, and microseismic (MS) monitoring were carried out to study the development and occurrence mechanisms of fault-slip rockburst. The fault-slip rockburst occurred in the hanging wall of a structure plane with dark green filling material and the rock mass slipped along the structure plane. It shows characteristic of intermittent occurrence, which results in great psychological pressure on workers. The dominant frequency of the rockburst MS event during the fault-slip rockburst is 13 Hz, which shows that the fault slip rockburst can be captured by the MS monitoring system. Extremely intense MS activity was recorded during the rockburst. The development and occurrence processes of the fault-slip rockburst were studied using this MS information. The stress evolution during the rockburst was studied by analyzing the dynamic stress drop. For the evolution mechanism of the fault-slip rockburst, many tensile fracture events occurred during the development stage, and a few shear fractures, corresponding to structure plane dislocation, occurred before the occurrence of the fault-slip rockburst. The presence of a large natural structure plane resulted in a higher stress and crack extension, and reduced the length of the penetration path, resulting in a stronger destructiveness. The results can be used for the further research on fault-slip rockbursts and planning appropriate warning and mitigation measures.

## Highlights

- An extremely intense fault-slip rockburst with local magnitude of 2.3 in a deep tunnel was introduced.
- Occurrence characteristics of fault-slip rockburst were analyzed.
- The development and occurrence mechanisms of the fault-slip rockburst including the fracture type and evolution mechanism, were studied.

**Keywords** Rock mechanics · Fault-slip rockburst · Microseismic (MS) monitoring · Structure plane · Deep tunnel

✉ Xia-Ting Feng  
fengxiating@mail.neu.edu.cn

<sup>1</sup> Key Laboratory of Ministry of Education On Safe Mining of Deep Metal Mines, Northeastern University, Shenyang 110819, China

<sup>2</sup> State Key Laboratory of Geomechanics and Geotechnical Engineering, Institute of Rock and Soil Mechanics, Chinese Academy of Sciences, Wuhan 430071, Hubei, China

## 1 Introduction

Rockburst is a dynamic disaster that commonly occurs during excavation in deep underground projects, threatens the safety of construction workers and equipment, delays the construction schedule, and leads to large economic losses. Rockburst is a sudden and violent release of elastic energy that has accumulated in rock masses (Feng et al. 2022; Leveille et al. 2017; Zhang et al. 2012; Zhao et al. 2018). According to the development mechanisms of rockbursts, they can be divided into strain rockburst, strain-structure

slip rockburst and fault-slip rockburst (Feng et al. 2019). Many studies on the mechanisms of the first two types of rockbursts have been carried out (Feng et al. 2012; Hoek et al. 1995; Hu et al. 2020; Jiang et al. 2020; Li et al. 2017; Xiao et al. 2016b). Research on the development mechanism of rockburst is the basis of not only the modelling, numerical simulation, and theoretical analysis of rockburst, but also the warning and mitigation of rockburst (Feng et al. 2015a), so studying the mechanism of fault-slip rockburst in hard tunnel projects is urgent and meaningful due to the increasing number of tunnel projects to be constructed and many faults in these areas.

Compared with strain rockburst and strain-structure slip rockburst, fault-slip rockburst occurs more suddenly, has a wider influence area and stronger destructiveness, and may even induce continuous intense rockburst, which can generally reach the earthquake level (Williams et al. 1992). For example, in South Africa, a fault-slip rockburst occurred with a local magnitude of 2.1 at a depth of 2300 m in the Carletonville gold mine area, and the stope was seriously damaged (Durrheim et al. 1998). Additionally, more than one thousand fault-slip rockbursts have occurred at the Witwaterstand gold mine (Li et al. 2018). In China, the recorded fault-slip rockburst case with the highest magnitude is the fault-slip rockburst that occurred in the Qianqiu coal mine with a magnitude of 4.1 (energy of  $3.5 \times 10^8$  J) on November 3, 2011 (Cai et al. 2014).

There have been many studies on the mechanism of fault slip using theoretical models (Scholz 1998), laboratory tests (Kato et al. 1999), numerical simulations (Manouchehrian and Cai 2018) and field monitoring in mines (Lu et al. 2019; Snelling et al. 2013). In 1966, Brace and Byerlee (1966) found that stick-slip accompanied frictional slipping in laboratory experiments, and proposed that the stick-slip model can be used to describe the occurrence of shallow earthquakes. Then, the stick-slip model was introduced into the study of the occurrence mechanism of fault-slip rockburst in coal mines (Qi et al. 1995). Many researchers have studied rock friction by performing laboratory tests to determine the mechanism of earthquakes and rockbursts caused by fault slip (Deng et al. 2018; Zhao et al. 2020). Direct shear friction slipping tests on granodiorite have revealed the intermittent slipping characteristics of fault slip evolution, and that the slip distance and velocity at the first slip are both greater than those at the second slip (Song et al. 2011). Shear stress decreases during fault slip, showing an obvious stress drop in laboratory tests (Kato et al. 1999). The effects of fault parameters on fault-slip rockburst at the intersection of a longwall coal panel and a fault have been investigated (Jiang et al. 2019). These studies clarified the fault slip process and revealed the occurrence mechanism of fault-slip rockburst at the laboratory test scale to a certain extent. In addition, some studies have revealed the characteristics of fault-slip

rockburst in coal mines. However, the development and occurrence mechanisms of fault-slip rockburst in hard rock engineering situ have not been revealed, especially in deep hard rock tunnels, and further research is needed.

Microseismic (MS) signals reflect a considerable amount of rockburst information, such as the rock failure mechanism and rockburst development processes (Feng et al. 2012, 2021; Xiao et al. 2016a; Younga and Collinsb 2001). Therefore, MS monitoring technology can be used to analyze the rock fracture mechanism and the development process of rockburst in deep tunnels to study the mechanism of fault-slip rockburst. In this work, we introduced a case study of an extremely intense fault-slip rockburst with a local magnitude of 2.3 (energy of  $1.8 \times 10^8$  J) in a deep tunnel. The rockburst caused a large economic loss and delayed the construction schedule for nearly 2 months. Then, the development and occurrence mechanisms of the fault-slip rockburst in deep tunnels were explored by combining in-situ failure analysis, geological survey and MS information, i.e., the frequency spectral characteristics, the spatial and temporal evolution characteristics of the MS activity, dynamic stress drop and rock fracture type.

## 2 The “2018.11.15” Fault-Slip Rockburst

### 2.1 Engineering Background

The deep tunnel studied in this paper was constructed for a high-elevation railway, located in southwestern China. The trend of the tunnel is  $104^\circ$ , and the total length is 13,073 m (Fig. 1a). Most of the tunnel is in medium-grained biotite monzogranite (E2R), and locally, the tunnel crosses small pegmatite vein ( $\rho$ ). The geologic structures in this area are well-developed. The tunnel passes through the Zangmu fault at DK200+006, with a nearly vertical bandwidth of 30–50 m. The elevation in the construction zone is 3260–5500 m. The maximum burial depth of the tunnel is 2080 m. From DK 190+408~195+605 and DK 200+335~203+455, the tunnel consists of a main tunnel and a parallel pilot. At the rest of the chainage, a single main tunnel was excavated (Fig. 1b). The section size of the main tunnel is 8.62 m  $\times$  7.3 m (Fig. 1c), and it was excavated by drilling and blasting. The uniaxial compressive strength of the granite is approximately 160 MPa.

The in-situ stress measurements collected by the Northwest Research Institute of China Railway Engineering Corporation (Xinjiang branch) using the hollow inclusion gauge method show that the principal stresses at DK 194+200 (with a depth of 1446 m) are 49.7 MPa, 37.0 MPa, 36.1 MPa (Zhang et al. 2020). The maximum principal stress at the tunnel is subhorizontal with an azimuth angle of  $197.9^\circ$  and

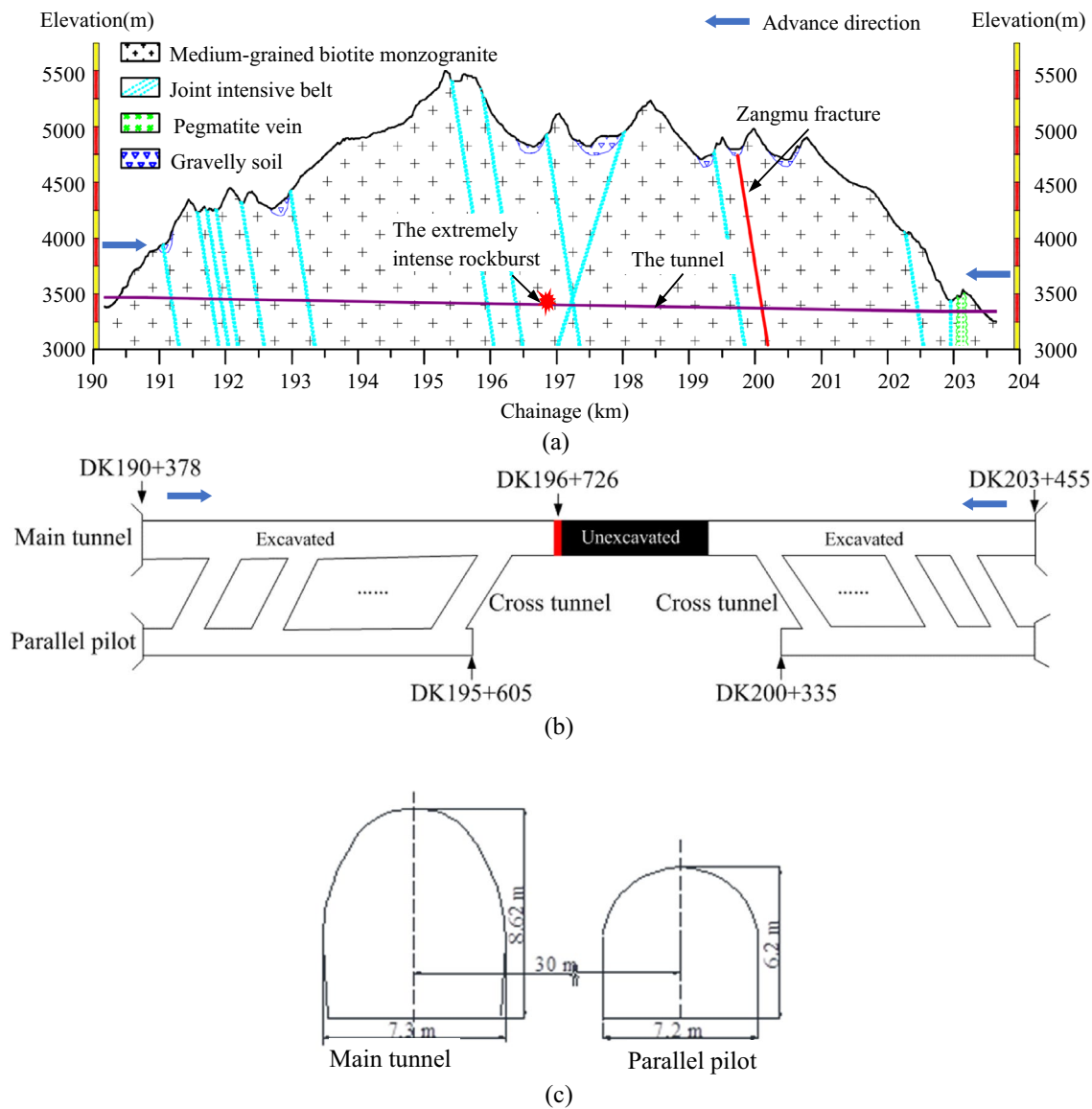


**Fig. 1** Engineering background of the deep tunnel in southwestern China. **a** Vertical cross-section along the tunnel (Hu et al. 2020), **b** layout of the tunnel, and **c** section profile of the tunnel

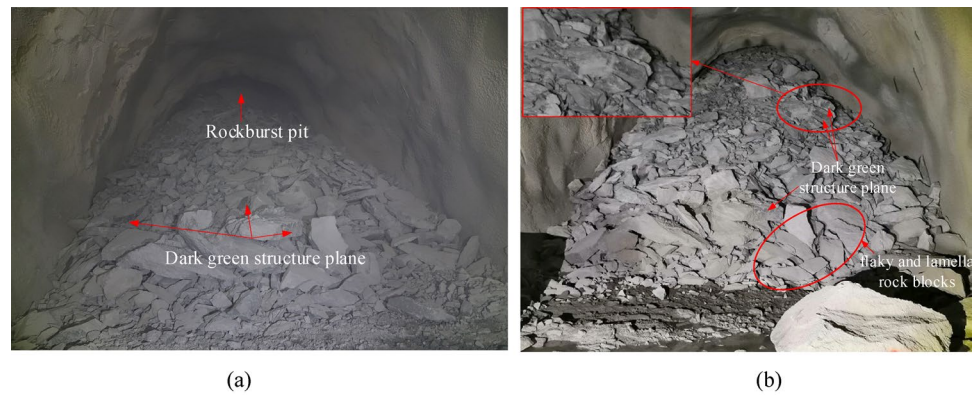
a dip angle of  $2.3^\circ$ , which is approximately perpendicular to the tunnel.

## 2.2 The Occurrence Situations of the Rockburst

During the excavation of the tunnel, an extremely intense rockburst occurred at DK 196+720~196+725 on November 15, 2018 (Fig. 1). At 7:33 in the morning, excavation blasting in the working face was carried out normally, then transported out rock blocks and eliminated risk. At approximately 12:00, an extremely intense rockburst occurred at the vault behind the working face (the working face was at DK 196+726). The main rockburst occurred at approximately 13:00. Loud crackling noise like a blasting and

muffled noise were heard. Many rock blocks suddenly slipped down, and quickly filled the 20 m zone behind the working face (Fig. 2a). As the rockburst continued, the rockburst pit was filled by the rockburst blocks (Fig. 2b). Until November 17, the working face became basically stable, and rockburst stopped. The rock masses in the rockburst zone were transported out at 12:00–18:00 on November 17 and 8:00–16:00 on November 18. Then, rockburst started again at 6:29 on November 19. Loud sounds were heard. Until 12:00 on November 20, the rockburst zone became stable again, and the rockburst ended. The positions of these two rockbursts were the same, and the second rockburst extended deep to the surrounding rock from the first rockburst pit. Therefore, these two rockbursts were the two occurrence

**Fig. 2** Photographs of the evolution of the extremely intense rockburst. **a** The overall condition of the rockburst pit on November 15, 2018, and **b** the rockburst pit on November 16, 2018



processes of the extremely intense rockburst. The two rockbursts are described as rockburst I and rockburst II. Sketches of the evolution of the rockburst pit are shown in Fig. 3. The depth of the rockburst pit after rockburst I was approximately 8–9 m (Fig. 3a, b), and the depth after rockburst II was approximately 11–13 m (Fig. 3c, d). The volume of the bursting rock mass was estimated to be 900 m<sup>3</sup>.

The rockburst produced blocky, flaky, grainy, and powdery rock fragments. Figure 2 also shows that there were many flaky and thin sheet like rock fragments, with thicknesses of 1–2 cm. Figure 4a shows a larger rock block with a size of 2.3 m × 1.6 m × 0.53 m (length × width × thickness). These rock blocks were fresh and not weathered. In addition,

dark green structure surfaces were found in many larger rock blocks, as shown in Fig. 2. After the large rocks were transported out, a large amount of rock grains and dark green rock powder were observed in the rockburst pit (Fig. 4b).

After the occurrence of rockburst II, construction remained paused for five days until the environment was completely calm, and rock blocks cleaning started on November 25, 2018. The rockburst was treated until January 7, 2019. That is, the construction schedule was delayed by 52 days. In addition, many support materials were consumed during the rockburst treatment process, including 1080 bolts, 27 steel arches, 80 pipe sheds, steel fiber-reinforced concrete and many steel meshes. These materials increased the large economic loss caused by the rockburst.

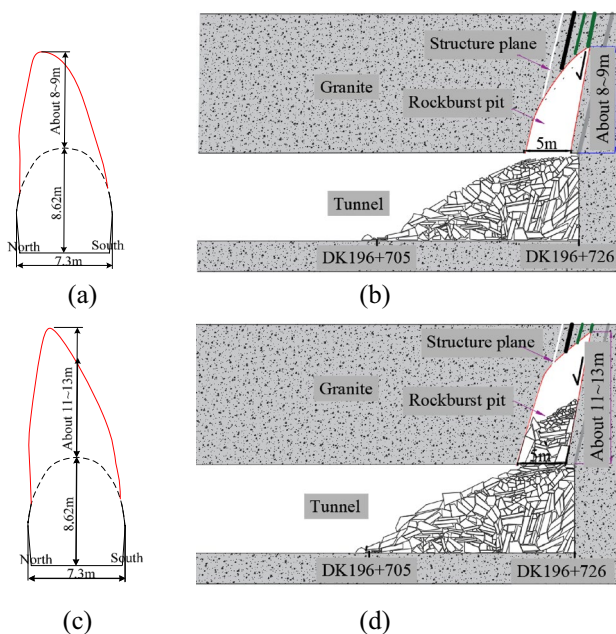


**Fig. 3** Evolution sketches of the rockburst pit during the rockburst. **a** Cross-section of the rockburst pit after rockburst I, **b** front view of the rockburst pit after rockburst I, **c** cross-section of the rockburst pit after rockburst II, and **d** front view of the rockburst pit after rockburst II

### 2.3 Geological Surveys in the Rockburst Zone

A geological survey was carried out in the rockburst zone. Several structure planes were developed approximately perpendicular to the excavation direction of the working face, as shown in Figs. 5, 6 and Table 1. These structure planes are a set of joints distributed behind the working face (1st joint set), from DK 196 + 721 ~ DK 196 + 725, including structure planes 1#–5#. The dip direction of the structure planes is 280° and the corresponding dip angle is 70°–90°. Among these structure planes, the 1# structure plane is rigid, straight, smooth, and unfilled. The 2# structure plane is crooked, rough, opened and partially filled with black powder to a thickness of 50 mm. The 3# structure plane is straight and filled with a green filling to a thickness of 3 mm. The 4# structure plane is slightly opened and partially filled with dark green filling. The filling thickness is 20 mm. The 5# structure plane is crooked, closed and includes white quartz vein filling to a thickness of 40 mm. In addition, a joint set is distributed on the north side of the working face (2nd joint set) (see Fig. 6f), with a dip direction of 10° and a dip angle of 70°. These joints are open, with no observable filling and no weathering.

**Fig. 4** Shape of rock blocks from the rockburst. **a** A large rock block with a size of 2.3 m × 1.6 m × 0.53 m, and **b** rock grains and dark green rock powders



In addition, the revealed 4# structure plane was surveyed after the fault-slip rockburst. Component analysis shows that the dark green filling material is formed by chloritization of biotite and feldspar. Many dark green slip failure surfaces were observed in the rockburst blocks (see Fig. 7a). An SEM test was conducted on the dark green failure surfaces. The

scanning results show a linear small granular pattern and a stripe pattern at location 1 and location 2 (see Fig. 7b, c), which are typical failure modes of shear slip. The rock grains and powders at the rockburst pit were produced by slipping friction along the dark green failure surfaces during the rockburst. Therefore, this rockburst is a fault-slip rockburst that occurred at the 4# dark green structure plane and slipped down along the structure plane.

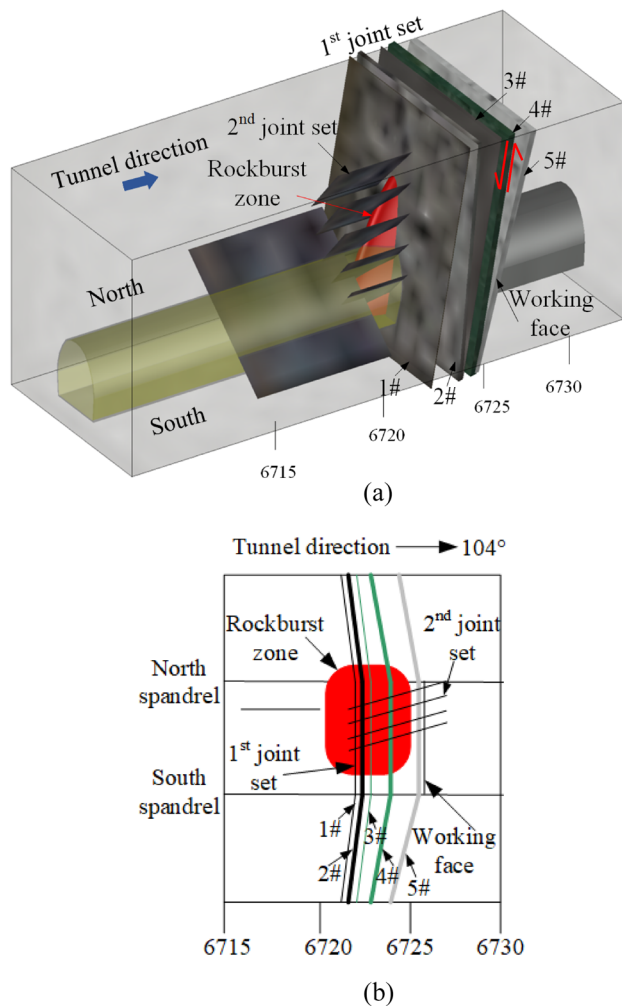


**Fig. 5** Sketches of the engineering geology in the rockburst zone. **a** Structure planes and rockburst pit in the rock mass, and **b** geological spread map exposed at the tunnel surface

### 3 In Situ MS Monitoring of the Fault-Slip Rockburst

#### 3.1 MS Monitoring Scheme

To monitor frequently occurring rockbursts in the deep tunnel of the study area, an MS monitoring system was installed in April 2017 (Hu et al. 2020; Niu et al. 2020). The layout of the MS monitoring system is shown in Fig. 8a. The system was composed of a monitoring center, sensors, several communication elements (wireless bridges), junction boxes, cables, etc. Two rows were set up with eight uniaxial sensors (Fig. 8b) with four sensors installed at each row. The sensors had an approximate usable frequency range that varied from 7 to 2000 Hz (with a sensitivity of 80 V/ms), and the sampling frequency was set to 6 kHz. Installation methods of sensors, wave velocity model, wave velocity inversion method, arrival time picking method, etc., have been studied previously (Feng et al. 2015b; Xiao et al. 2015; Zhang et al. 2021). Some MS parameters, such as MS energy, dynamic stress drop, and local magnitude are used in this paper, which can be obtained with seismological methods (Andrews 1986; Gibowicz 1998; Gibowicz et al. 1991; Mori 2003).

#### 3.2 The Spectral Characteristics of MS Events During the Fault-Slip Rockburst

The MS monitoring system captured the whole development and occurrence processes of the extremely intense

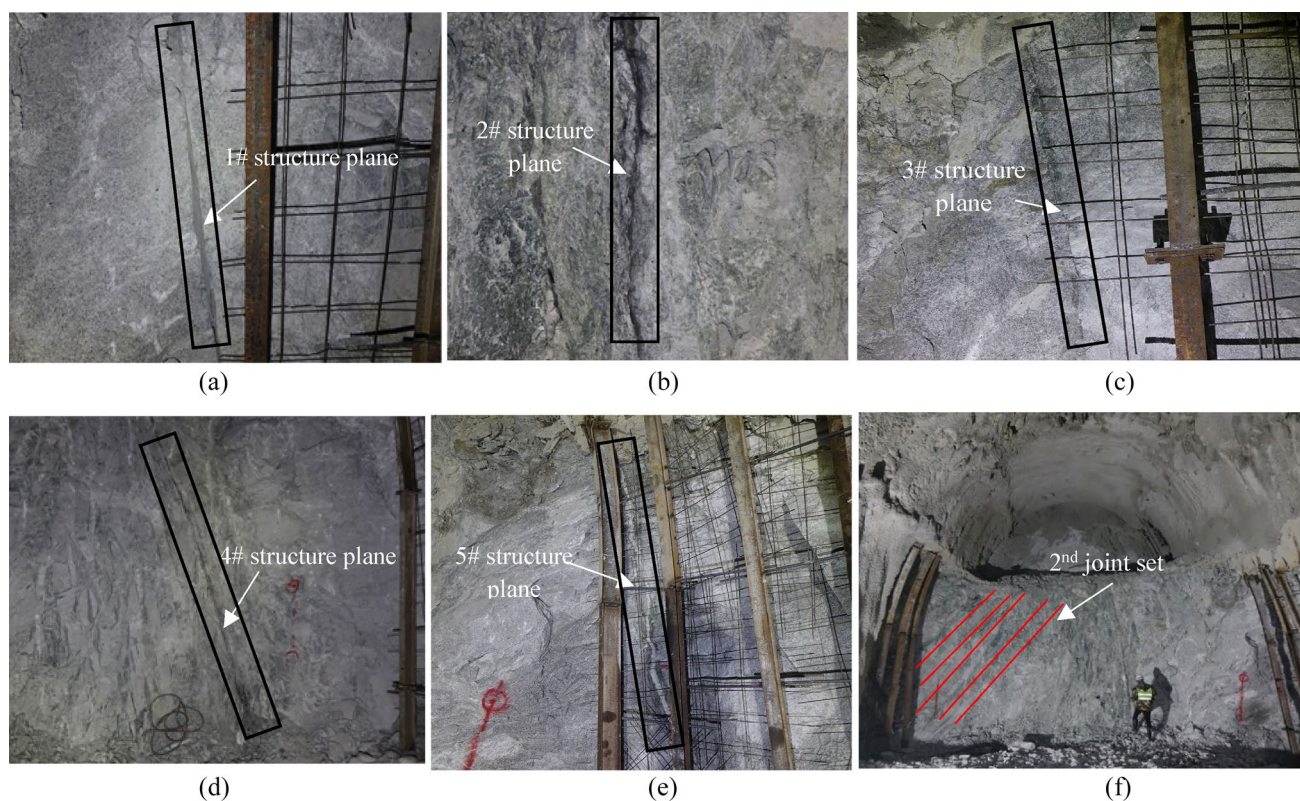


**Fig. 6** The structure planes exposed by tunnel excavation at the rockburst zone. **a** 1# structure plane, **b** 2# structure plane, **c** 3# structure plane, **d** 4# structure plane, **e** 5# structure plane, and **f** 2nd joint set at the north side of working face

**Table 1** The orientation and property of the observed structure planes

| Joint set     | Structure plane    | Property                                      | Filling thickness (mm) | Dip direction (°) | Dip angle (°) |
|---------------|--------------------|---|------------------------|-------------------|---------------|
| 1st joint set | 1# structure plane | Straight, smooth, unfilled                    | –                      | 280               | 80            |
|               | 2# structure plane | Crooked, rough, black powder filling, opened  | 50                     | 280               | 90            |
|               | 3# structure plane | Straight, green filling                       | 3                      | 280               | 80            |
|               | 4# structure plane | Straight, dark green filling, slightly opened | 20                     | 280               | 70            |
|               | 5# structure plane | Crooked, white quartz vein filling, closed    | 40                     | 280               | 70            |
| 2nd joint set |                    | Opening, no filling or weathering             | –                      | 10                | 70            |

fault-slip rockburst. One MS event with the highest MS energy was captured at 13:03:41 when the main rockburst occurred, which was the rockburst MS event. The local magnitude of the event reached 2.3, with an MS energy of  $1.8 \times 10^8$  J. Notably, the local magnitude of the blasting event at 7:33 was just 1.6, with an MS energy of  $2.2 \times 10^7$  J. The energy of the rockburst event was eight times that of the blasting event. Figure 9 shows some waveforms and their spectra of the rockburst MS event. The amplitudes of the MS waveforms are all greater than  $2 \times 10^{-2}$  m/s, and the maximum amplitude reaches  $5.07 \times 10^{-2}$  m/s at the G3 sensor (Fig. 9a). Xiao et al. (2015) measured the amplitude

of rock mass fracture events to be  $10^{-7}$ – $10^{-2}$  m/s in tunnels with the same layout of sensors excavated by drilling and blasting. Therefore, the waveform amplitude during the rockburst is a relatively large value in terms of the statistical results of other rock fracture events in tunnels excavated by drilling and blasting. The frequency spectra of these waveforms are shown in Fig. 9b. The dominant frequency of these waveforms is 13 Hz.

The evolution of the spectral characteristics of the rock fracture signals collected by the G2 sensor during the fault-slip rockburst was analyzed, as shown in Fig. 10. During the development process of the fault-slip rockburst, the

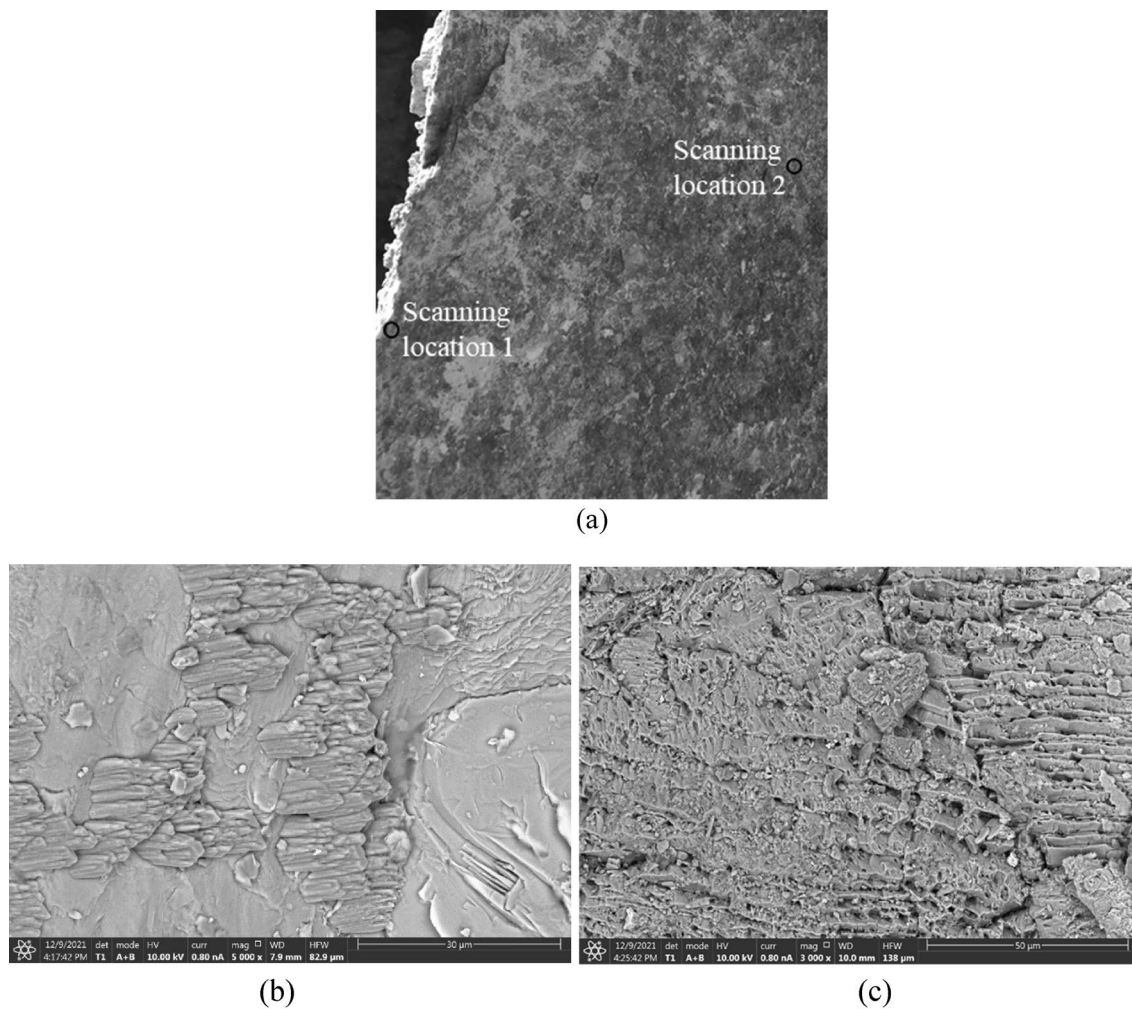


**Fig. 7** The revealed slip failure surface and its scanning results of 4# structure plane after the fault-slip rockburst. **a** The revealed slip failure surface and the scanning location, **b** the scanning result of location 1, and **c** the scanning result of location 2

dominant frequency is mainly distributed from 180 to 190 Hz. When the fault-slip rockburst is about to occur, the main frequency gradually decreases, and the dominant frequency is 13 Hz when the rockburst occurs, a relatively low value, but it is still within the acquisition range of the sensors.

### 3.3 The MS Evolution During the Fault-Slip Rockburst

The spatial distribution characteristics of MS events with MS energies larger than 1 J during the “2018.11.15” fault-slip rockburst are shown in Fig. 11. Figure 11a–e shows the MS event spatial distribution characteristics during the development stage with different distances  $L$  from the working face to 4# structure plane. A negative distance indicates that the working face is close to the 4# structure

plane but has not yet passed through the structure plane. A positive distance indicates that the working face has passed through the 4# structure plane. Figure 11f–h shows the MS event spatial distribution characteristics during the occurrence stages of the rockburst. The color of the spheres represents the occurrence time of the MS events and size represents the logarithm of the MS energy. The MS events associated with the development and occurrence of fault-slip rockburst are selected by the pink rectangular area, i.e., the rockburst zone, which was determined by the spatial distribution studies about the rockbursts and the MS activity in tunnels (Zhao et al. 2013). The total width of the rectangular area is 35 m. Since the excavation process is from the hanging wall to the footwall of the structure plane, and microseismic events are mostly distributed in the hanging wall, 25 m among the rectangular area is in the hanging wall and 10 m is in the footwall. The dip angle is

**Fig. 8** Layout of the MS monitoring system. **a** Overall layout, and **b** sensor arrangement in three-dimensional space (Hu et al. 2020)

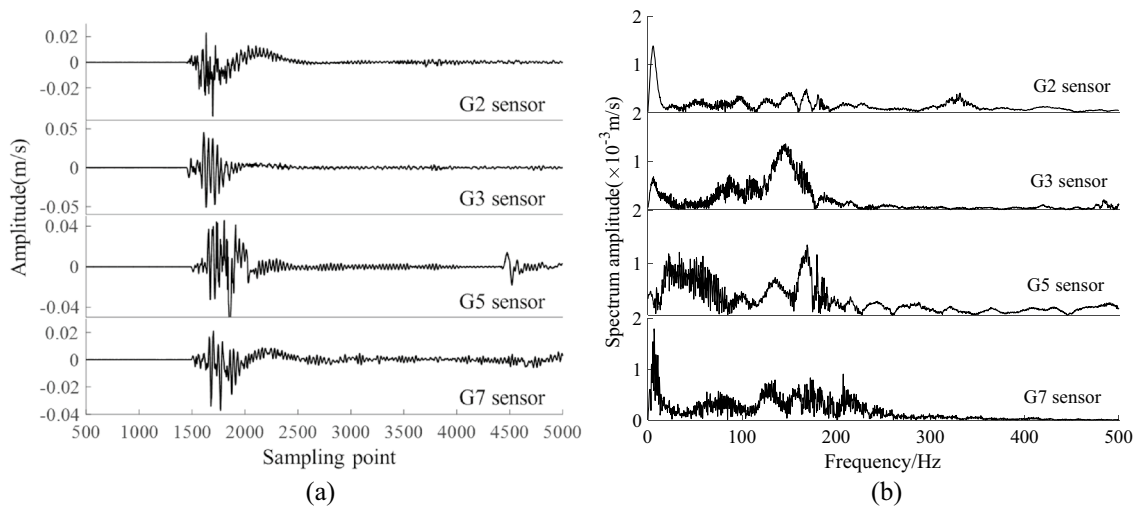
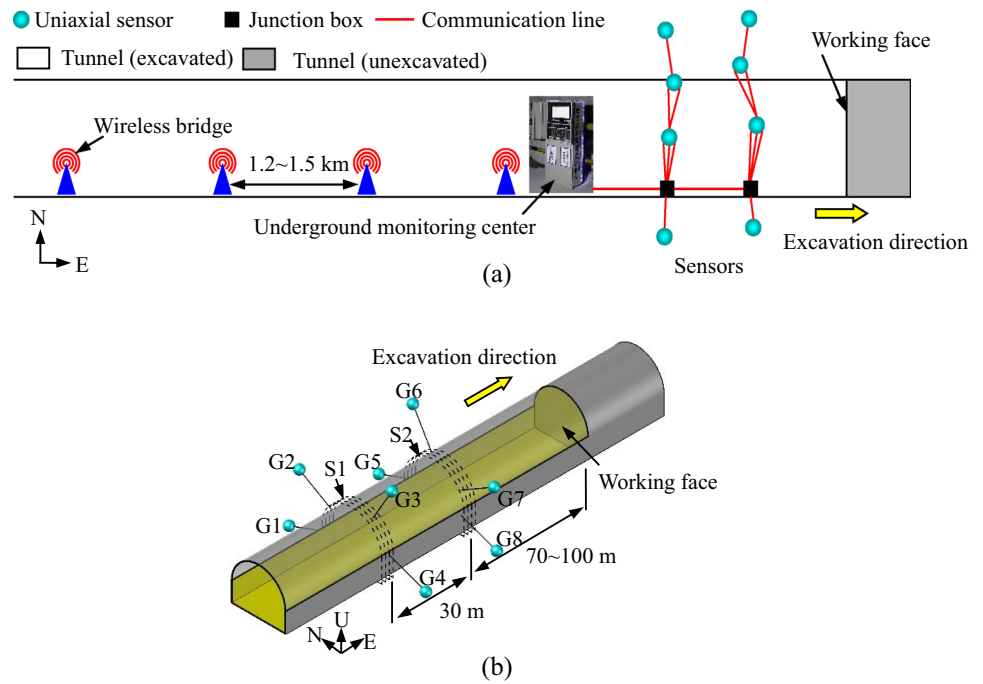


**Fig. 9** The **a** MS waveforms and **b** frequency spectra of the rockburst event with the greatest MS energy

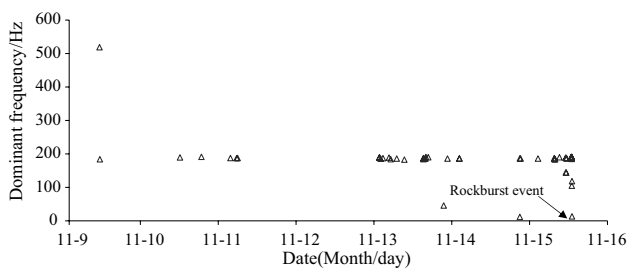


**Fig. 10** The dominant frequency of rock fracture waveforms during the development of the fault-slip rockburst

80°, the same as the 4# structure plane. The occurrence of the first rock fracture event (observed in the rockburst zone at 11:26:01 on November 9, 2018) can be considered the start of the development stage of the rockburst.

As Fig. 11a–e shows, during the development of the fault-slip rockburst, the spatial distribution characteristics of the MS events vary. When the distance from the working face to 4# structure plane was far, the MS events were mainly distributed around the tunnel and closed to the working face. As the distance from the working face to 4# structure plane decreased, more MS events occurred and accumulated



together in the hanging wall of the structure plane. When the distance was 1 m, most MS events were distributed in the hanging wall of the structure plane. During this process, the MS events expanded upwards gradually to 22 m above the tunnel. Even some MS events were distributed within 30–40 m above the tunnel.

The fault-slip rockburst has experienced the process of rockburst occurrence (rockburst I), rockburst stopped temporarily and rockburst reoccurrence (rockburst II). Figure 11f–h shows the MS event spatial distribution characteristics at these stages. We can see that most of the MS events clustered along the structure plane during the first occurrence of rockburst. Many MS events were distributed on the structure plane, including the greatest rockburst MS event (see Fig. 11f). The clean-up of the rockburst blocks slightly disturbed the surrounding rock and caused the reoccurrence of rockburst. Therefore, the time from 8:00, November 17 to 4:00, November 19 can be seen the development of rockburst II. Some rock fracture events occurred distributed at the hanging wall of 4# structure plane (see Fig. 11g). Then, from 5:00 to 16:00 on November 19, 173 MS events were recorded with a cumulative logarithmic energy of 6.33, distributed in the range of 9–20 m above the tunnel along the structure plane (Fig. 11h).

The above analysis shows that the studied rockburst developed from the hanging wall of the structure plane and expanded along the structure plane. Rock mass fracturing was initially distributed on the surface of tunnel surrounding rock, then gradually expanded upwards along the structure plane to 22 m above the tunnel. Some rock mass fractures were distributed within 30–40 m above the tunnel. These results show that a high rockburst risk still existed in the hanging wall of the structure plane. Fortunately, the waiting time for rockburst II was long. If there is construction disturbance again before the MS activity has stopped completely, rockburst is likely to occur again.

### 3.4 The Dynamic Stress Drop During the Fault-Slip Rockburst

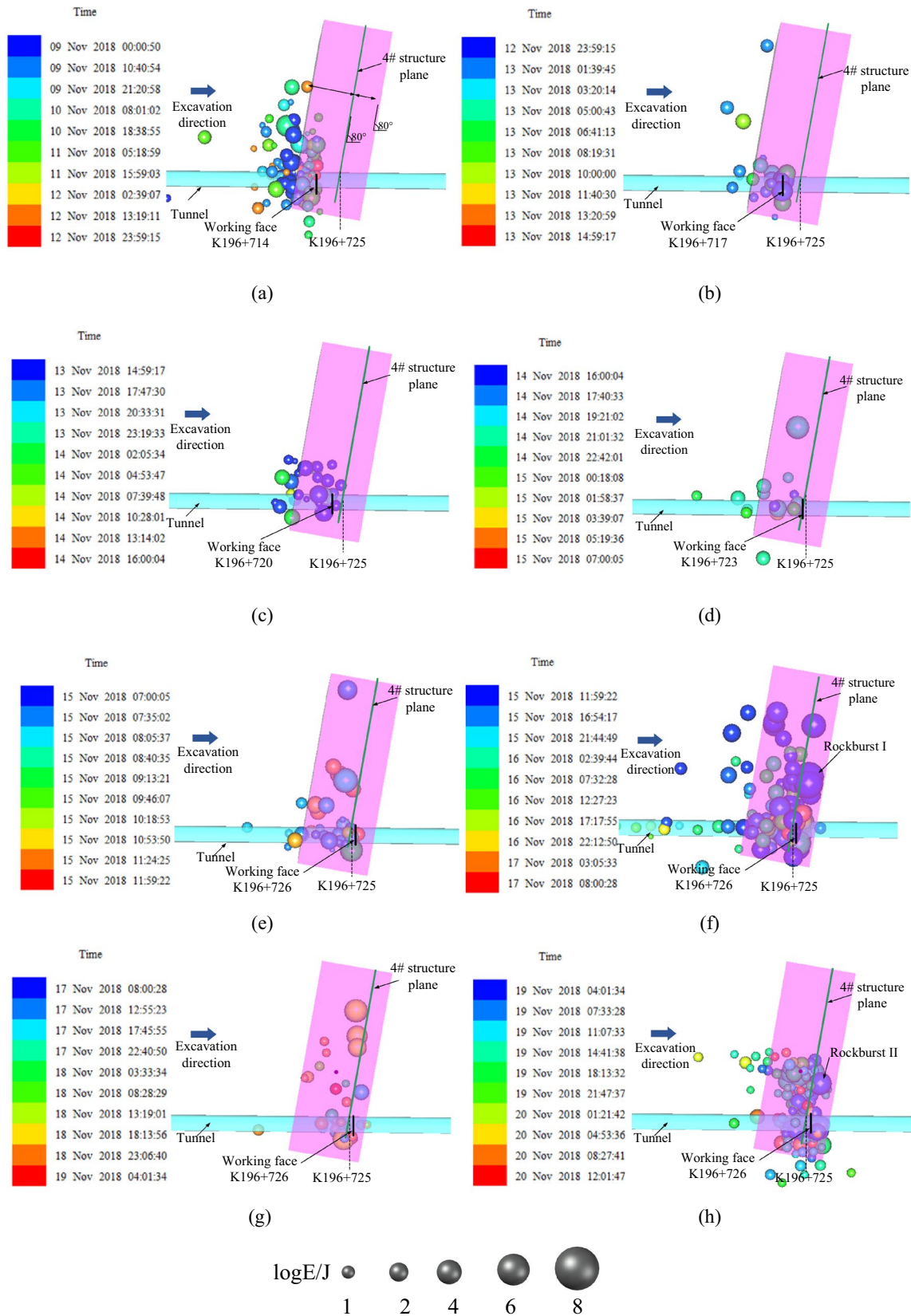
The dynamic stress drop is an important parameter during the process of fault slip. For a tensile fracture in an intact rock mass, the dynamic stress drop is the stress released on the fracture surface when the rock mass fractures. For fault slip, the dynamic stress drop is the stress difference before and after fault slip. The greater the dynamic stress drop is, the higher the stress in the environment where the rock mass is located, and the more likely severe shear instability (Deng et al. 2018; Ryder 1988), so the dynamic stress drop can be used to describe the stress level on the structure plane and in the surrounding rock (Ruff 1999). The dynamic stress drop can be obtained through MS monitoring. Therefore, the distribution and evolution characteristics of the dynamic

stress drop during the fault-slip rockburst were analyzed (see Figs. 12, 13). Figure 12a–e shows the dynamic stress drop during the development stage under different distances from the working face to 4# structure plane. Figure 12f–h shows the dynamic stress drop during the occurrence stage of the rockburst. The Z-axis coordinates denote the system elevation set by the MS monitoring system; a Z coordinate of 0 m represents an altitude of 3414 m.

As Figs. 12a–e and 13 show, during the development stage, the largest values of dynamic stress drop were 1.92 MPa, 3.06 MPa, 1.88 MPa, 12.7 MPa and 6.92 MPa, when the distances were  $-26 \sim -11$  m,  $-8$  m,  $-5$  m,  $-2$  m, and 1 m, respectively. The dynamic stress drop increased gradually as the working face approached approximately 2 m from the structure plane, at which point the dynamic stress drop decreased slightly with decreasing distance from the structure plane. Regarding the distribution characteristics, the dynamic stress drop concentrated around the tunnel and closed to the working face with a larger distance. Then, it concentrated in the hanging wall of the structure plane with decreasing distance from the structure plane. Figure 14 shows the evolution of the dynamic stress drop at the measurement points during the development of the fault-slip rockburst with different distances from the working face to 4# structure plane. Measurement points  $A_1$ – $G_1$  are distributed in the hanging wall of the structure plane, with a horizontal distance of 5 m from the structure plane. They are distributed 2 m below the tunnel and 2 m, 12 m, 22 m, 32 m, 42 m, and 52 m above the tunnel. Measurement points  $A_2$ – $G_2$  are distributed at the footwall of the structure plane at the same distance. These figures also show that when the working face approached the structure plane, the stress near the structure plane gradually increased and that when the working face passed through the structure plane, the stress gradually decreased.

Figures 12f–h and 13 show that the maximum dynamic stress drop is 12.7 MPa and 16.94 MPa during the development and occurrence stage of rockburst I. It is 9.1 MPa at the development stage of rockburst II. A relatively high value shows that the energy has not been released completely. The maximum dynamic stress drop is 9.8 MPa during the occurrence stage of rockburst II. The above analysis shows that the dynamic stress drop is higher at the occurrence stage than at the development stage. It at rockburst I is higher than that at rockburst II. The concentration area of the dynamic stress drop at the occurrence stage is closer to the structure plane, or at the structure plane.

Here, the stress evolution during the development of fault-slip rockburst was discussed in terms of the distribution characteristics and evolution of the dynamic stress drop (Fig. 15). When the working face approaches the structure plane, the stress concentration area gradually approaches to the structure plane and the stress value increases gradually.



◀**Fig. 11** Evolution of the distribution of the MS events during the fault-slip rockburst with different distances  $L$  from the working face to 4# structure plane. **a**  $L = -26 \sim -11$  m, **b**  $L = -8$  m, **c**  $L = -5$  m, **d**  $L = -2$  m, **e**  $L = 1$  m, **f** rockburst occurrence ( $L = 1$  m), **g** rockburst stopped temporarily ( $L = 1$  m), and **h** rockburst recurrence ( $L = 1$  m). A negative distance indicates that the working face is close to 4# structure plane but has not yet passed through the structure plane. A positive distance indicates that the working face has passed through the 4# structure plane

Extremely high stress concentrates in the hanging wall of the structure plane when the distance is small. The stress  $\sigma_d$  is the superposition of the stress  $\sigma_e$  in front of the tunnel caused by excavation and the tectonic stress  $\sigma_s$  related to the structure plane. Then, the stress decreases slightly when the working face passes through the structure plane.

### 3.5 The Development and Occurrence Processes of the Fault-Slip Rockburst Using MS Information

As shown in Fig. 16, the evolution of the MS activity with MS energies greater than 1 J in the pink rectangular rockburst zone was analyzed to reveal the development and occurrence processes of the fault-slip rockburst. Every point shows the MS activity that occurred at the rockburst zone in 4 h. The development process of fault-slip rockburst was revealed by the development stage of rockburst I, and the time from the first rock fracture event in the rockburst zone to rockburst I occurred (11:26 on November 9 ~ 12:00 on November 15). In this stage, the working face maintained normal construction operations, so the development stage is described below in terms of areas divided by a certain distance from the working face to 4# structure plane, which can be summarized as follows:

1. Slow development (distance from  $-26$  to  $-11$  m): The MS activity increased slowly. The greatest number of MS events observed was 17, and the mean number observed was 2.75. These MS events mainly occurred after blasting and were distributed around the tunnel and close to the working face. The greatest logarithm of MS energy observed was 4.3, and most logarithms of MS energy observed were less than 4. The maximum dynamic stress drop was 1.5 MPa.
2. Fast development (distance from  $-11$  to  $-2$  m): The MS activity increased rapidly. The greatest number of MS events observed was 14, and the mean number observed was 3.69. A few MS events were distributed near the structure plane. The greatest logarithm of MS energy observed was 6.44 and most logarithms of MS energy observed were 4–5. The maximum dynamic stress drop was 13 MPa.

3. Imminent rockburst (distance from  $-2$  to 1 m): The MS activity increased sharply. 34 MS events occurred with a logarithm of MS energy of 6.42 from 7:33 to 12:00 after blasting at 7:33 on November 15, distributed in the hanging wall along the structure plane. The maximum dynamic stress drop was 6.5 MPa. Violent MS activity indicated that the structure plane would slip and that the fault-slip rockburst would occur soon.

The development stage of fault-slip rockburst is divided into three stages according to the MS activity. In fact, the strength and evolution process of MS activity correspond to the process of crack evolution. The stronger the MS activity is, the faster the crack generation and propagation. Therefore, these three stages correspond to the stages of crack initiation, propagation and penetration respectively.

The whole fault-slip rockburst process can be divided into four stages (no change in distance in the later stage, instead it is expressed by time), i.e., the development stage of rockburst I, occurrence stage of rockburst I, development stage of rockburst II and occurrence stage of rockburst II, which are expressed by stages ①–④ (Fig. 16). Here, the MS activities that occurred in the four stages were analyzed (Fig. 17).

Figure 17a shows that the energy (logarithm values) of MS events is mainly distributed at  $(-2, 7)$  and that the majority of the MS events are distributed at  $(-1, 4)$ , accounting for 85.7% of all the MS events. Eight MS events have energies larger than 6. Among them, five MS events occurred at the occurrence stage of rockburst I, and one occurred at the occurrence stage of rockburst II. The remaining two MS events occurred at the development stage of rockburst I (occurring at the fast development stage and imminent rockburst stage). A total of 110 MS events occurred with energies within  $(3, 6)$ . A total of 29.1% and 45.5% of them occurred at the development and occurrence stages of rockburst I, respectively. A total of 5.4% and 20% of the MS events occurred at the development and occurrence stages of rockburst II, respectively. The number of high-energy MS events at the occurrence stage is greater than that at the development stage. In addition, Fig. 17b shows that the proportion of high-energy events at rockburst I is greater than that at rockburst II. Regarding the accumulated MS energy, the logarithms are 6.77, 8.43, 6.15, and 6.41 at the four stages of the studied rockburst (Fig. 17b). The accumulated MS energy at the occurrence stage is higher than that at the development stage, which is 45 and 3.4 times at the two rockbursts. The total energy during rockburst I was 44.7 times that during rockburst II.

Considering the rockburst occurrence conditions and MS monitoring results, this fault-slip rockburst has the characteristics of intermittent occurrence, and its energy

**Fig. 12** Distribution characteristics of dynamic stress drop during the fault-slip rockburst with different distance  $L$  from the working face to 4# structure plane. **a**  $L = -26 \sim -11$  m, **b**  $L = -8$  m, **c**  $L = -5$  m, **d**  $L = -2$  m, **e**  $L = 1$  m, **f** rockburst occurrence ( $L = 1$  m), **g** rockburst stopped temporarily ( $L = 1$  m), and **h** rockburst reoccurrence ( $L = 1$  m)

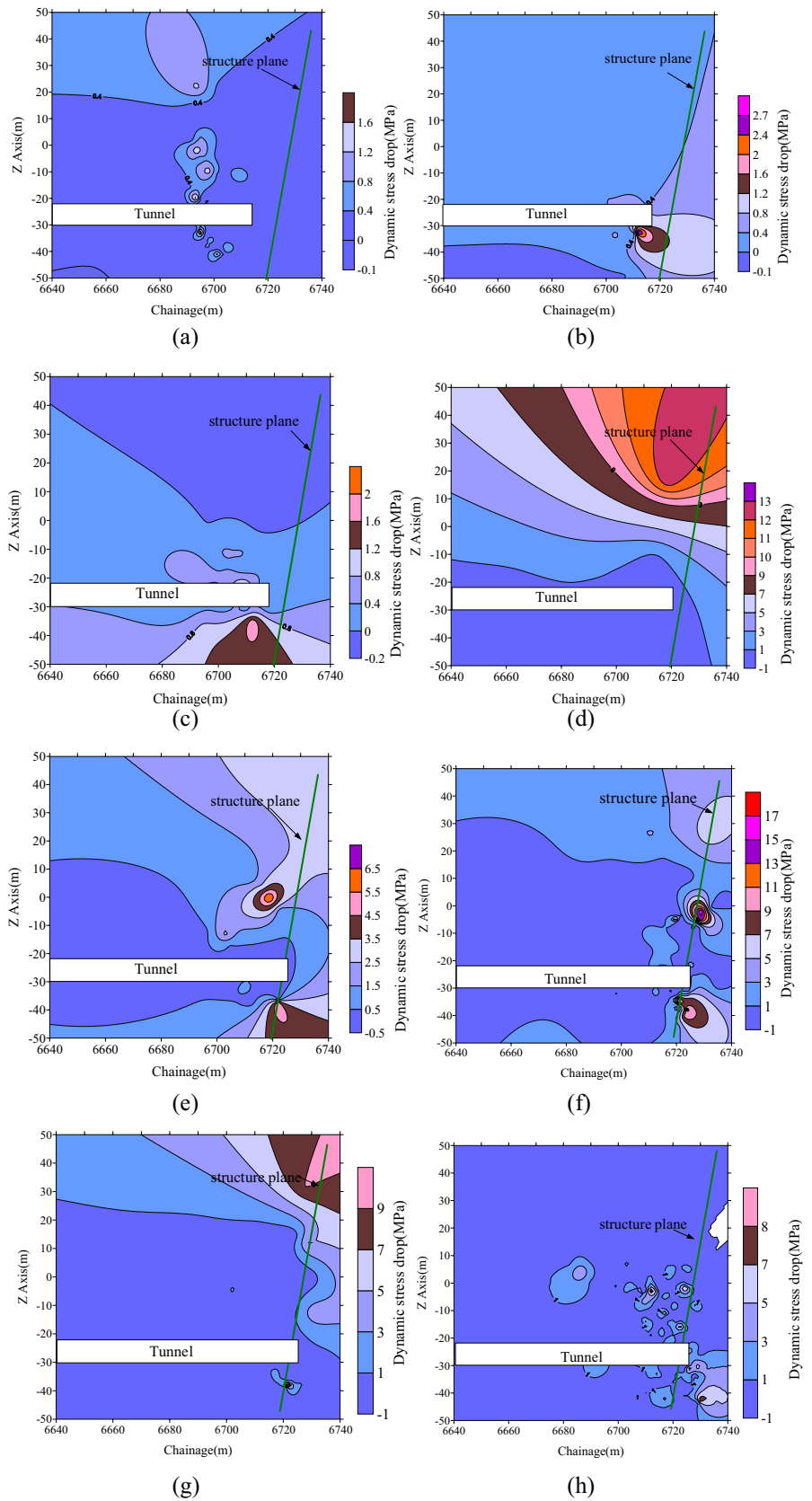
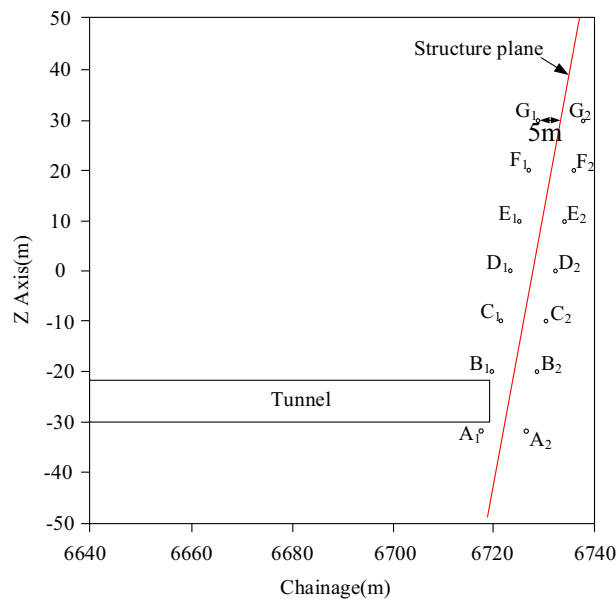
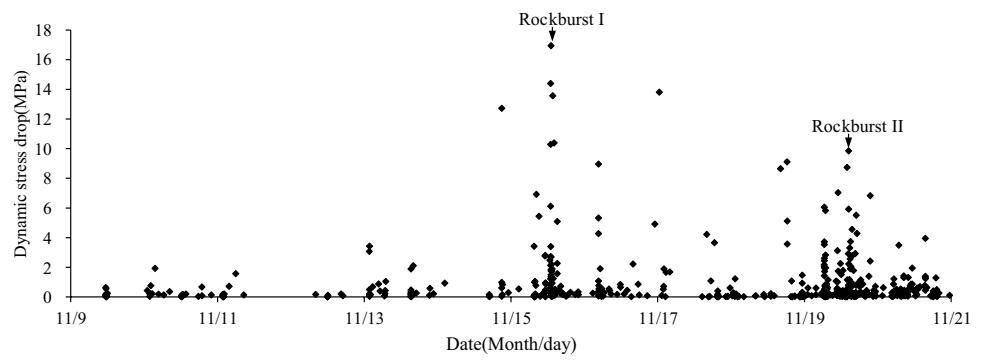
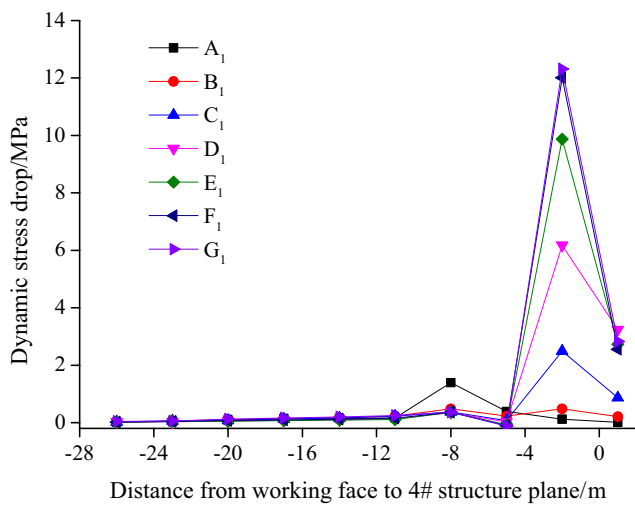


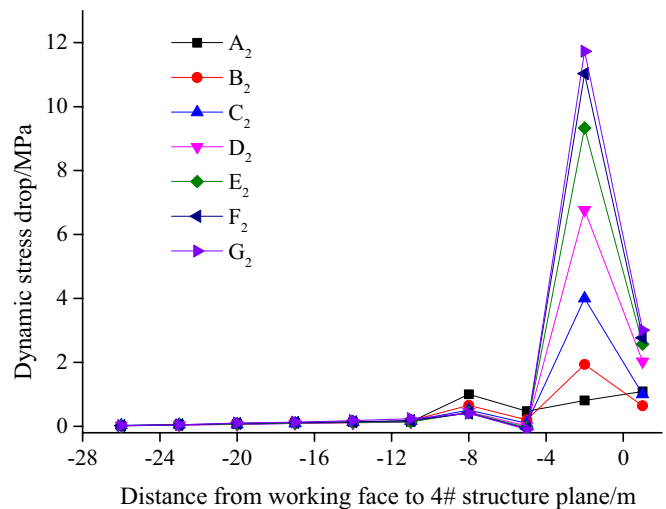
**Fig. 13** Evolution of the dynamic stress drop during the fault-slip rockburst



(a)



(b)



(c)

**Fig. 14** The evolution of the dynamic stress drop at measurement points during the development of the fault-slip rockburst. **a** The arrangement of the measurement points. **b** The dynamic stress drop in the hanging wall. **c** The dynamic stress drop at the footwall

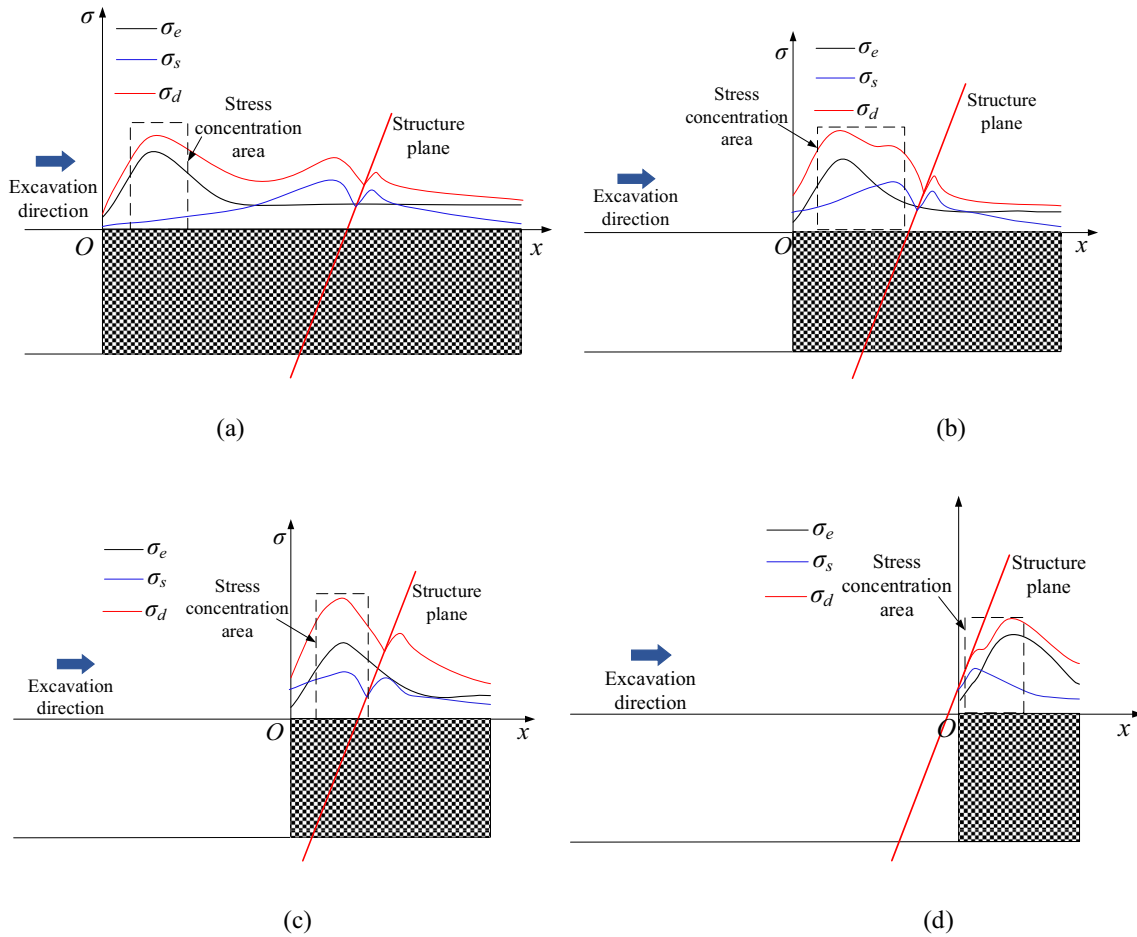


**Fig. 15** Stress evolution sketches in the hanging wall of the structure plane during the development of the fault-slip rockburst. The stress is **a** lower when the distance from the working face to the structure plane is farther, **b** increases since the stress superposition as the working face approaches the structure plane, **c** extremely concentrates

in the hanging wall of the structure plane when the working face is nearly to the structure plane, and **d** slightly reduced when the working face passes the structure plane.  $\sigma_e$  denotes the stress in front of the tunnel caused by excavation,  $\sigma_s$  denotes the tectonic stress related to the structure plane, and  $\sigma_d$  is the superposition of the two stresses

**Fig. 16** Evolution of the number and energy of the MS events during the fault-slip rockburst

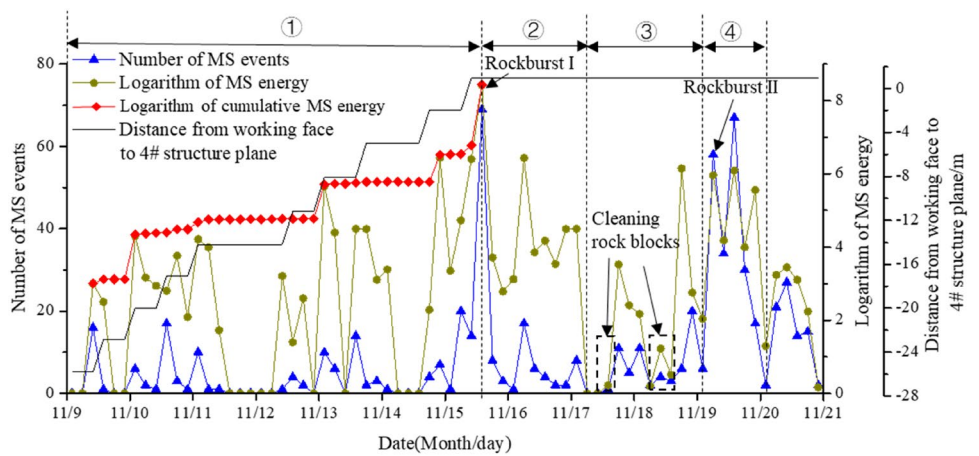
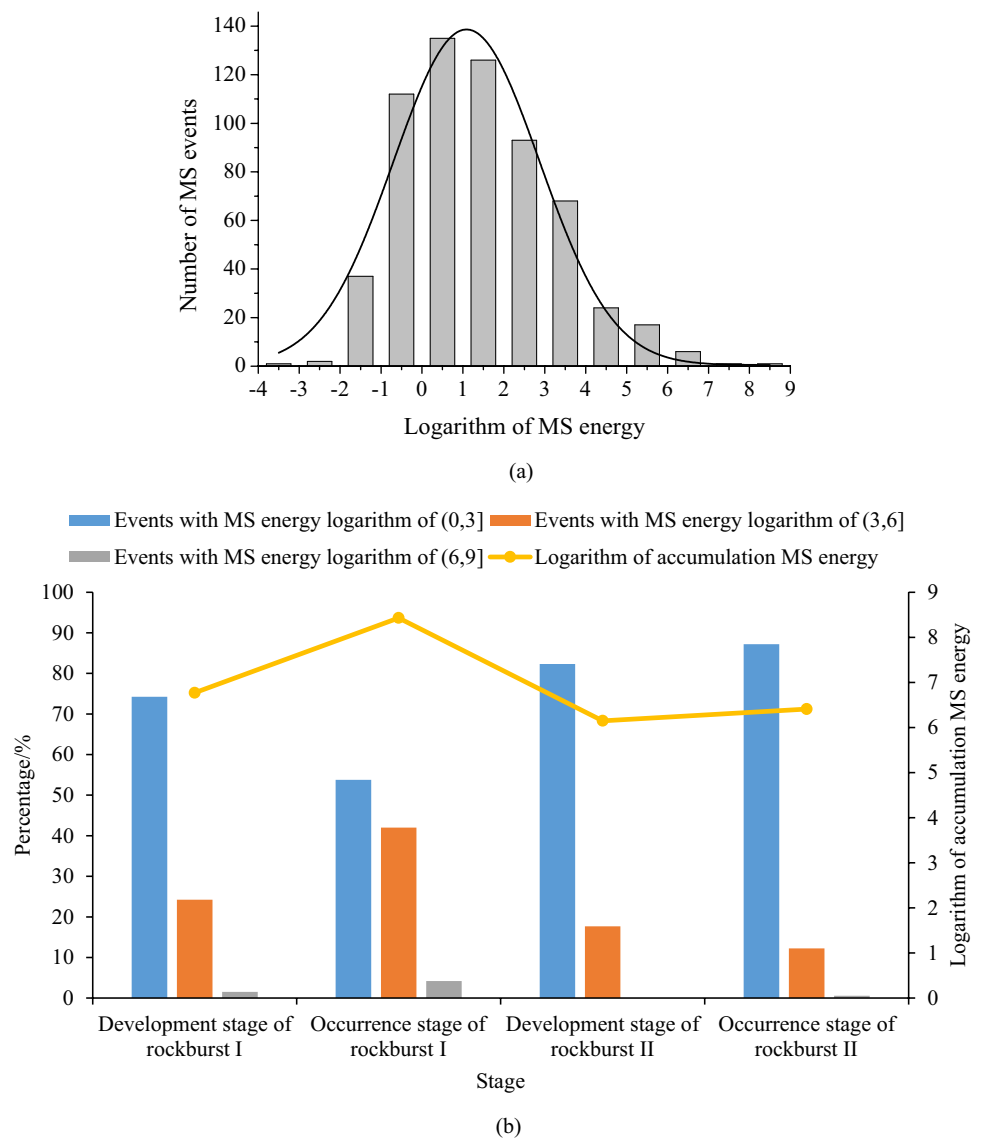


**Fig. 17** MS activity during the fault-slip rockburst. **a** The number of MS events with different logarithms of MS energy, and **b** the energy distribution at different stages



is also intermittently released. This is consistent with previously presented stick slip model results (Scholz 1998), laboratory testing results (Song et al. 2011) and MS monitoring results in mines (Lu et al. 2018). In addition, the energy released during the first fault slip is greater than that at the second time, as observed during laboratory testing (Song et al. 2011). The first violent rockburst easily results in a large-scale disaster, and the second rockburst will also result in great psychological pressure on workers. The dynamic stress drop is often used to predict the occurrence of aftershocks in seismology (Mori 2003). This parameter may play an important role in the warning of fault-slip rockburst, and it can be used to analyze whether rockburst will reoccur.

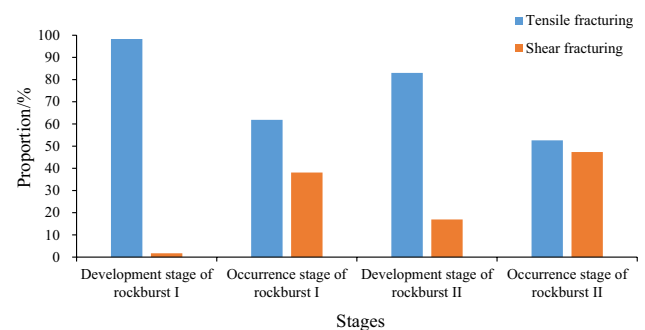


**Fig. 18** The proportion of rock fracture types at the different stages during the fault-slip rockburst

## 4 The Mechanism of the Fault-Slip Rockburst

### 4.1 Rock Fracture Mechanism During the Fault-Slip Rockburst

To study the fracture mechanism of rock fracture events, Xiao et al (2016b) proposed the method of P-wave development. In this method, the relative development degree of P-wave is characterized by the strength of the first motion amplitude of the P-wave relative to the overall microseismic waveform. The P-wave development degree  $P_D$ , is defined as:

$$P_D = \sum_{i=1}^N A_p^i / A_M^i \quad (1)$$

where  $N$  is the number of trigger sensors of the microseismic event,  $A_p^i$  is the first motion amplitude of the P-wave recorded by the  $i$  triggering sensor, and  $A_M^i$  is the maximum amplitude of the waveform recorded by the  $i$  triggering sensor. The criterion for determining the focal mechanism based on the P-wave development of microseismic events is shown in formula (2)

$$\begin{cases} P_D \geq 0.047 & \text{Tensile failure} \\ P_D < 0.047 & \text{Shear failure} \end{cases} \quad (2)$$

The P-wave development degree of MS events with energies larger than 1 J associated with the fault-slip rockburst was calculated. According to the criterion, the proportions of the fracture types of the MS events associated with the fault-slip rockburst at different stages are shown in Fig. 18. The rock fracture events during the rockburst development stages are mainly tensile fractures, approximately 98.3% and 83%, respectively for the two rockbursts. The proportions of shear fracture events during the rockburst development stage are just 1.7% and 17% at rockbursts I and II, respectively. During the rockburst occurrence stage, the proportions of shear fracture events increase to 38.1% and 47.4% at the two rockbursts. The tensile fracture events decrease to 61.9% and 52.6% at rockbursts I and II respectively.

The mechanism evolution of the rock mass fracture associated with the fault-slip rockburst is shown in Fig. 19. Combining the above analysis, the rock fracture events during the rockburst development stage are mainly tensile fractures. Shear and tensile fracture events occur alternately during the rockburst occurrence stage with similar proportions. In addition, some shear fracture events occur during the development stage before the occurrence of fault-slip rockburst, which shows that there was a small amount of shear slip before the fault-slip rockburst occurred. These shear fracture events were distributed near or on the structure plane. The SEM test results on the failure surfaces also show the failure mode of shear slip along the structure plane (see Fig. 7b, c).

### 4.2 The Evolution Mechanism of the Fault-Slip Rockburst

The evolution mechanism of the “2018.11.15” fault-slip rockburst was deduced by analyzing the failure characteristics, geological conditions, and MS monitoring results. Figure 20 shows a conceptual model that was used to simulate the evolution mechanism of the fault-slip rockburst. The spatial characteristics of the MS events show that the fault-slip rockburst occurred in the hanging wall of the structure plane. Therefore, the right boundary of the rockburst was controlled by the steeply inclined structure plane filled with dark green filling material.

Due to the influences of engineering excavation, high geostress, and the structure plane, a stress concentration area forms in the surrounding rock. When the distance from the working face to the structure plane is farther, rock fracture occurs around the tunnel and close to the working face under high stress. Cracks are sporadically generated in the hanging wall of the structure plane. The fractures in this area are basically tensile fractures and cracks parallel to the tunnel are formed. This stage corresponds to the slow development stage (Fig. 20a).

As the working face approaches the structure plane, the stress concentration area is gradually closed to the structure plane and the stress increases gradually (Fig. 15a, b). A large number of cracks are generated in the hanging wall. The fractures in this stage are also mainly tensile (Fig. 20b).

**Fig. 19** Evolution of the rock mass fracture mechanism during the fault-slip rockburst

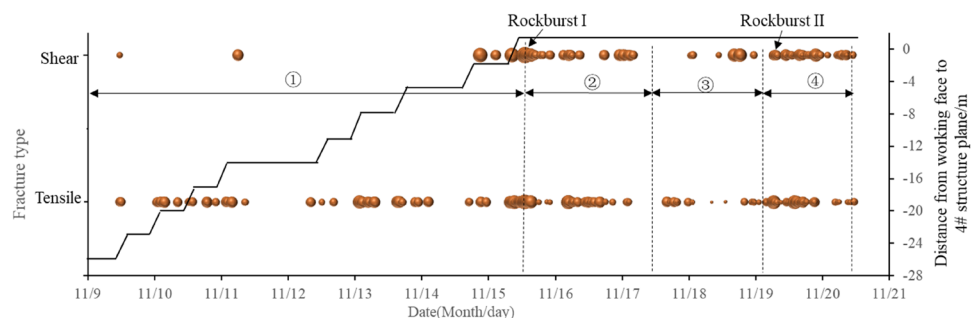
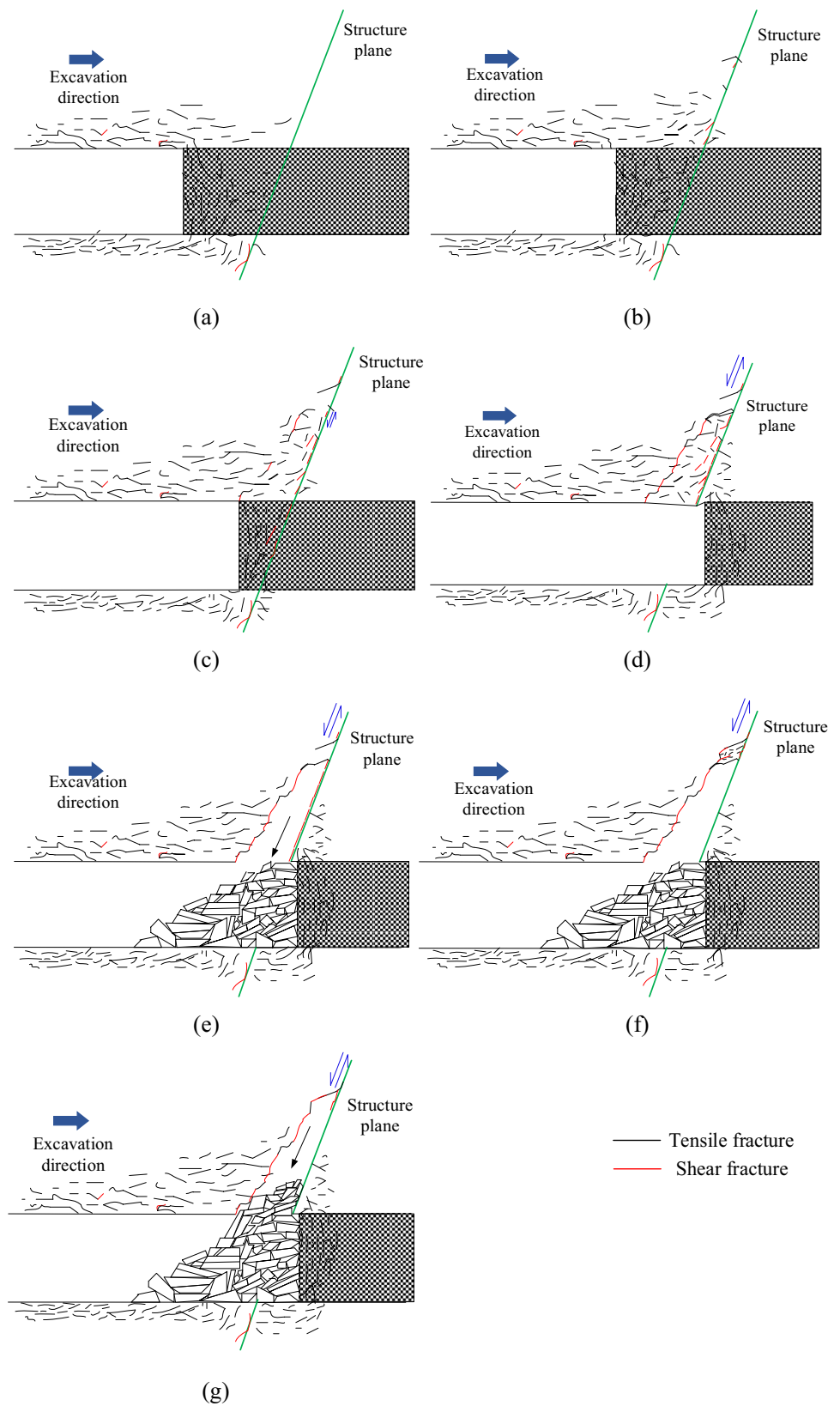




**Fig. 20** Conceptual model simulating the fault-slip rockburst. **a** Cracks generate sporadically in the hanging wall of the structure plane when the distance from the working face to the structure plane is far, **b** a large number of cracks generate in the hanging wall due to the higher stress as the working face approaches the structure plane, **c** cracks extend due to the dislocation of the structure plane and the higher stress when the working face approaches the structure plane further, **d** cracks penetrate the structure plane, **e** rockburst occurs along the structure plane, **f** cracks extend upwards again under the slight disturbance, and **g** rockburst occurs again



As the working face further approaches the structure plane, the superposition of the stress  $\sigma_e$  and the tectonic stress  $\sigma_s$  leads to an extremely high stress  $\sigma_d$  in the hanging wall of the structure plane (Fig. 15c). Many tensile fractures occur, forming transverse cracks parallel to the tunnel. The high stress also leads to a few rock mass dislocations in the hanging wall along the structure plane and further results in many longitudinal tensile cracks parallel to the structure plane in the hanging wall, which gradually extend deep and connect with the transverse cracks along the direction parallel to the structure plane (Fig. 20c). These two stages correspond to the fast development stage.

When the working face passes through the structure plane, under the influence of excavation disturbance and high stress, the rock masses in the hanging wall of the structure plane have a downwards slip trend. Rock fractures develop rapidly. The cracks extend rapidly and are completely connected with the structure plane. A certain amount of mixed and shear fractures occur in this stage (Fig. 20d). This stage corresponds to the imminent rockburst stage. Then, the fault-slip rockburst occurs (Fig. 20e). The transverse cracks resulted in many flakey and sheet-like rock fragments observed in the blasted rock mass (Fig. 2a, b). The rock grains and dark green rock powders are signs of slip caused by shear movement (Fig. 4b). After the main rockburst, new cracks initiate, propagate, penetrate, and slip along the structure plane. Therefore, many mixed and shear fractures occur, with a similar proportion of tensile fractures.

As the waiting time of rockburst increases, the MS activity tends to be gentle. However, the energy accumulated in the hanging wall of the structure plane is not fully released. Under the influence of slight construction disturbance, the dislocation of the structure plane results in crack extension again. These cracks, parallel to the structure plane, penetrate the transverse cracks (Fig. 20f), resulting in the occurrence of rockburst II (Fig. 20g).

In conclusion, during the development process of fault-slip rockburst, the structure plane plays an important role. The stress level in the hanging wall of the structure plane is further improved by the tectonic stress, leading to more tensile fractures, forming transverse cracks parallel to the tunnel. The cohesion of the structure planes is relatively low and even loses cohesion under excavation disturbance, so the structure plane is easily dislocated. The dislocation results in the formation of longitudinal tensile cracks parallel to the structure plane. These cracks extend until they penetrate with free surface, and then eject and slip along the free surface. Different from strain rockburst, the free surface of fault-slip rockburst is a pre-existing large natural structure plane. Therefore, under the same conditions, the penetration path of fault-slip rockburst is less than that of strain rockburst. Coupled with the complex stress environment, this finding explains why the destructiveness of fault-slip

rockburst is greater than that of strain rockburst and strain-structure plane rockburst.

## 5 Conclusions

In this work, an extremely intense fault-slip rockburst that occurred in a deep tunnel in southwestern China was introduced. The rockburst caused a large economic loss and delayed the construction schedule for nearly 2 months. The development mechanism and occurrence process of fault-slip rockburst were studied by in-situ failure analysis, geological surveys, and MS monitoring. The fault-slip rockburst occurred in the hanging wall of the dark green structure plane and slipped along the structure plane. The local magnitude of the fault-slip rockburst was 2.3, and the MS energy was  $1.8 \times 10^8$  J. The frequency spectral analysis shows that the main frequency gradually decreases when the fault-slip rockburst is about to occur, and the main frequency is 13 Hz when the rockburst occurs, which is within the acquisition range of the sensors.

The MS monitoring results show extremely intense MS activity during the fault-slip rockburst. During the development stage, the fractures in the rock mass gradually expanded upwards along the structure plane to 22 m above the tunnel, and some fractures are distributed within 30–40 m, reflecting a higher rockburst risk in the hanging wall of the structure plane. This fault-slip rockburst occurs intermittently, and its energy is also intermittently released, which results in great psychological pressure on workers. The logarithm of the accumulated MS energy reaches 6.77, 8.43, 6.15, and 6.41 at the development and occurrence stages of rockburst I and II, respectively. In addition, the dynamic stress drop was used to study the stress state during the development and occurrence of the fault-slip rockburst. Furthermore, the dynamic stress drop can be used as an indicator in the warning system of fault-slip rockburst and in the analysis of whether rockburst will reoccur.

The rock fracture events that occur during the rockburst development stage are mainly tensile fractures, and a few shear fracture events occur before the occurrence of fault-slip rockburst. These shear fracture events are the dislocation signal of the structure plane. The structure plane plays an important role during the fault-slip rockburst at the fast development stage. The stress in the hanging wall of the structure plane is further improved by the tectonic stress, leading to more transverse cracks parallel to the tunnel. The dislocation of structure plane causes longitudinal tensile cracks. These cracks extend parallel to the structure plane until they penetrate the structure plane, forming rock fragments and resulting in the slip. The pre-existing large natural structure plane reduces the length of the penetration path,

leading to a stronger destructiveness. The results of this case study can be used as a basis for further mechanism research on fault-slip rockburst and planning appropriate warning and mitigation measures.

**Acknowledgements** The authors gratefully acknowledge financial support from the National Natural Science Foundation of China under Grant no. 51839003, the 111 Project under Grant no. B17009 and the Liao Ning Revitalization Talents Program under Grant no. XLYCYSZX1902.

## References

- Andrews DJ (1986) Objective determination of source parameters and similarity of earthquakes of different size. *Geophys Monogr* 37(6):259–267
- Brace WF, Byerlee JD (1966) Stick-slip as a mechanism for earthquakes. *Science* 153(3739):990–992
- Cai W, Dou LM, Li ZL, He J, He H, Ding YL (2014) Mechanical initiation and propagation mechanism of a thrust fault: a case study of the Yima Section of the Xiashi-Yima Thrust (North Side of the Eastern Qinling Orogen, China). *Rock Mech Rock Eng* 48(5):1927–1945. <https://doi.org/10.1007/s00603-014-0666-x>
- Deng SX, Li J, Jiang HM, Wang MY (2018) Experimental and theoretical study of the fault slip events of rock masses around underground tunnels induced by external disturbances. *Eng Geol* 233:191–199. <https://doi.org/10.1016/j.enggeo.2017.12.007>
- Durrheim RJ, Haile A, Roberts MKC, Schweitzer JK, Spottiswoode SM, Klokow JW (1998) Violent failure of a remnant in a deep South African gold mine. *Tectonophysics* 289:105–116
- Feng XT, Chen BR, Li SJ, Zhang CQ, Xiao YX, Feng GL, Zhou H, Qiu SL, Zhao ZN, Yu Y, Chen DF, Ming HJ (2012) Studies on the evolution process of rockbursts in deep tunnels. *J Rock Mech Geotech Eng* 4(4):289–295. <https://doi.org/10.3724/sp.J.1235.2012.00289>
- Feng GL, Feng XT, Chen BR, Xiao YX, Yu Y (2015a) A microseismic method for dynamic warning of rockburst development processes in tunnels. *Rock Mech Rock Eng* 48(5):2061–2076. <https://doi.org/10.1007/s00603-014-0689-3>
- Feng GL, Feng XT, Chen BR, Xiao YX, Jiang Q (2015b) Sectional velocity model for microseismic source location in tunnels. *Tunn Undergr Space Technol* 45(45):73–83. <https://doi.org/10.1016/j.tust.2014.09.007>
- Feng XT, Xiao YX, Feng GL, Yao ZB, Chen BR, Yang CX, Shao SG (2019) Study on the development process of rockbursts. *Chin J Rock Mech Eng* 38(4):649–673. <https://doi.org/10.13722/j.cnki.jrme.2019.0103>
- Feng XT, Yang CX, Kong R, Zhao J, Zhou YY, Yao ZB, Hu L (2021) Excavation-induced deep hard rock fracturing: methodology and applications. *J Rock Mech Geotech Eng*. <https://doi.org/10.1016/j.jrmge.2021.12.003>
- Feng GL, Chen BR, Xiao YX, Jiang Q, Li PX, Zheng H, Zhang W (2022) Microseismic characteristics of rockburst development in deep TBM tunnels with alternating soft–hard strata and application to rockburst warning: a case study of the Neelum-Jhelum hydropower project. *Tunn Undergr Space Technol* 122:104398. <https://doi.org/10.1016/j.tust.2022.104398>
- Gibowicz SJ (1998) Partial stress drop and frictional overshoot mechanism of seismic events induced by mining. *Pure Appl Geophys* 153:5–20. <https://doi.org/10.1007/s000240050182>
- Gibowicz SJ, Young RP, Talebi S, Rawlence DJ (1991) Source parameters of seismic events at the underground research laboratory in Manitoba, Canada—scaling relations for events with moment magnitude smaller than – 2. *Bull Seismol Soc Am* 81(4):1157–1182
- Hoek E, Kaiser PK, Bawden WF (1995) Support of underground excavations in hard rock. A. A. Balkema, Rotterdam
- Hu L, Feng XT, Xiao YX, Wang R, Feng GL, Yao ZB, Niu WJ, Zhang W (2020) Effects of structural planes on rockburst position with respect to tunnel cross-sections: a case study involving a railway tunnel in China. *Bull Eng Geol Environ* 79(2):1061–1081. <https://doi.org/10.1007/s10064-019-01593-0>
- Jiang LS, Kong P, Zhang PP, Shu JM, Wang QB, Chen LJ, Wu QL (2019) Dynamic analysis of the rock burst potential of a longwall panel intersecting with a fault. *Rock Mech Rock Eng* 53(4):1737–1754. <https://doi.org/10.1007/s00603-019-02004-2>
- Jiang JQ, Su GS, Zhang XH, Feng XT (2020) Effect of initial damage on remotely triggered rockburst in granite: an experimental study. *Bull Eng Geol Environ* 79(6):3175–3194. <https://doi.org/10.1007/s10064-020-01760-8>
- Kato N, Satoh T, Lei X, Yamamoto K, Hirasawa T (1999) Effect of fault bend on the rupture propagation process of stick-slip. *Tectonophysics* 310:81–99. [https://doi.org/10.1016/S0040-1951\(99\)00149-3](https://doi.org/10.1016/S0040-1951(99)00149-3)
- Leveille P, Sepehri M, Apel DB (2017) Rockbursting potential of kimberlite: a case study of diavik diamond mine. *Rock Mech Rock Eng* 3:1–9. <https://doi.org/10.1007/s00603-017-1294-z>
- Li TB, Ma CC, Zhu ML, Meng LB, Chen GQ (2017) Geomechanical types and mechanical analyses of rockbursts. *Eng Geol* 222:72–83. <https://doi.org/10.1016/j.enggeo.2017.03.011>
- Li P, Cai MF, Guo QF, Lu XG, Yan BQ (2018) Research situations and development tendencies of fault slip rockburst in coal mine. *J Harbin Inst Technol* 50(3):1–17
- Lu CP, Liu Y, Zhang N, Zhao TB, Wang HY (2018) In-situ and experimental investigations of rockburst precursor and prevention induced by fault slip. *Int J Rock Mech Min Sci* 108:86–95. <https://doi.org/10.1016/j.ijrmmms.2018.06.002>
- Lu CP, Liu B, Liu B, Liu Y, Wang HY, Zhang H (2019) Anatomy of mining-induced fault slip and a triggered rockburst. *Bull Eng Geol Environ* 78:5147–5160. <https://doi.org/10.1007/s10064-019-01464-8>
- Manouchehrian A, Cai M (2018) Numerical modeling of rockburst near fault zones in deep tunnels. *Tunn Undergr Space Technol* 80:164–180. <https://doi.org/10.1016/j.tust.2018.06.015>
- Mori J (2003) Stress drops and radiated energies of aftershocks of the 1994 Northridge, California, earthquake. *J Geophys*. <https://doi.org/10.1029/2001jb000474>
- Niu WJ, Feng XT, Xiao YX, Feng GL, Yao ZB, Hu L (2020) Identification of potential high-stress hazards in deep-buried hard rock tunnel based on microseismic information: a case study. *Bull Eng Geol Environ*. <https://doi.org/10.1007/s10064-020-01973-x>
- Qi QX, Liu TQ, Shi YW (1995) Mechanism of friction sliding instability of rock burst. *Ground Press Strata Control* 3–4:174–177
- Ruff LJ (1999) Dynamic stress drop of recent earthquakes: variations within subduction zones. *Pure Appl Geophys* 154:409–431. <https://doi.org/10.1007/s000240050237>
- Ryder JA (1988) Excess shear stress in the assessment of geologically hazardous situations. *J S Afr Inst Min Metall* 88(1):27–39
- Scholz CH (1998) Earthquakes and friction laws. *Nature* 391:36–42. <https://doi.org/10.1038/34097>
- Snelling PE, Godin L, McKinnon SD (2013) The role of geologic structure and stress in triggering remote seismicity in Creighton Mine, Sudbury, Canada. *Int J Rock Mech Min Sci* 58:166–179. <https://doi.org/10.1016/j.ijrmmms.2012.10.005>
- Song YM, Peng MS, Yang XB, Jiang YD (2011) Experimental investigation on instability transient process of fault rockburst. *Chin J Rock Mech Eng* 30(4):812–817. <https://doi.org/10.1007/s12583-011-0163-z>

- Williams TJ, Wideman CJ, Scott DF (1992) Case history of a slip-type rockburst. *PAGEOPH* 139(3/4):627–637. <https://doi.org/10.1007/BF00879955>
- Xiao YX, Feng XT, Hudson JA, Chen BR, Feng GL, Liu JP (2015) ISRM Suggested method for in situ microseismic monitoring of the fracturing process in rock masses. *Rock Mech Rock Eng* 49(1):343–369. <https://doi.org/10.1007/s00603-015-0859-y>
- Xiao YX, Feng XT, Feng GL, Liu HJ, Jiang Q, Qiu SL (2016a) Mechanism of evolution of stress–structure controlled collapse of surrounding rock in caverns: a case study from the Baihetan hydro-power station in China. *Tunn Undergr Space Technol* 51:56–67. <https://doi.org/10.1016/j.tust.2015.10.020>
- Xiao YX, Feng XT, Li SJ, Feng GL, Yu Y (2016b) Rock mass failure mechanisms during the evolution process of rockbursts in tunnels. *Int J Rock Mech Min Sci* 83:174–181. <https://doi.org/10.1016/j.ijrmms.2016.01.008>
- Younga RP, Collinsb DS (2001) Seismic studies of rock fracture at the Underground Research Laboratory, Canada. *Int J Rock Mech Min Sci* 38:787–799. [https://doi.org/10.1016/S1365-1609\(01\)00043-0](https://doi.org/10.1016/S1365-1609(01)00043-0)
- Zhang CQ, Feng XT, Zhou H, Qiu SL, Wu WP (2012) Case histories of four extremely intense rockbursts in deep tunnels. *Rock Mech Rock Eng* 45(3):275–288. <https://doi.org/10.1007/s00603-011-0218-6>
- Zhang W, Feng XT, Xiao YX, Feng GL, Yao ZB, Hu L, Niu WJ (2020) A rockburst intensity criterion based on the geological strength index, experiences learned from a deep tunnel. *Bull Eng Geol Environ* 79(7):3585–3603. <https://doi.org/10.1007/s10064-020-01774-2>
- Zhang W, Feng X, Bi X, Yao Z, Xiao Y, Hu L, Niu W, Feng G (2021) An arrival time picker for microseismic rock fracturing waveforms and its quality control for automatic localization in tunnels. *Comput Geotech* 135:104175. <https://doi.org/10.1016/j.compgeo.2021.104175>
- Zhao ZN, Feng XT, Chen BR et al (2013) Study of relativity between rockburst and MS activity zone in deep tunnel. *Rock Soil Mech* 34(2):491–497 ((in Chinese))
- Zhao TB, Guo WY, Tan YL, Yin YC, Cai LS, Pan JF (2018) Case studies of rock bursts under complicated geological conditions during multi-seam mining at a depth of 800 m. *Rock Mech Rock Eng* 51(5):1–26. <https://doi.org/10.1007/s00603-018-1411-7>
- Zhao YF, Jing G, Fan Y, Pan YS (2020) Experimental study on the microseism and charge signal time-frequency characteristics in the process of fault stick-slip instability. *Chin J Rock Mech Eng.* <https://doi.org/10.13722/j.cnki.jrme.2019.1025>

**Publisher's Note** Springer Nature remains neutral with regard to jurisdictional claims in published maps and institutional affiliations.